Measurement of far-infrared waveguide loss using a multisection single-pass technique

Michel Rochat,[a] Mattias Beck, and Jérôme Faist[b]
University of Neuchâtel, CH-2000 Neuchâtel, Switzerland

Ursula Oesterle
Swiss Federal Institute of Technology, CH-1015 Lausanne, Switzerland

(Received 7 November 2000; accepted for publication 29 January 2001)

Waveguide loss measurements based on a multisection single-pass technique have been performed for both mid-infrared and far-infrared quantum cascade structures. The far-infrared quantum cascade structures are based on a vertical transition active region emitting at $\lambda \approx 76\ \mu$m, embedded in a double-plasmon waveguide. The measured waveguide loss of $42 \pm 20\ \text{cm}^{-1}$ agrees well with the calculated one based on free carrier absorption. © *2001 American Institute of Physics.*
[DOI: 10.1063/1.1357444]

In the mid-infrared, lasers using the quantum cascade (QC) technology have been demonstrated[1] and are showing high operating performances and wide spectral emission possibilities (3.4–19 μm).[2,3] Although various research groups have shown far-infrared (FIR) electroluminescence in QC structures,[4–7] laser action could not be demonstrated so far using this technology. In order to reach laser threshold, an active region with a population inversion together with an efficient resonator designed for far-infrared wavelengths is needed. In the mid-infrared, good resonators are obtained by growing low refractive index claddings below and above the high refractive index active region. This can be done by molecular beam epitaxy as the needed cladding thickness is at least in the order of $\lambda/2$ in the material. In the far-infrared, however, waveguides based on pure dielectric confinement would require cladding thickness on the order of 10 μm. This technological difficulty can be avoided by using a metal instead of dielectrics for the mode confinement. This technique was first used with QC structures by Sirtori *et al.* in a waveguide based on surface plasmons.[8] Compared to waveguides based on dielectric confinement, this technique allows a drastic reduction of the cladding thickness, but results in a higher waveguide loss as the mode penetrates partly into the metal. However, these waveguides achieve larger overlap factor, ($\Gamma \approx 70\%$) than a regular slab waveguide ($\Gamma \approx 40\%$) with the same thickness of the waveguide core.

Our FIR waveguide is based on a metal–dielectric–metal, or double plasmon confinement commonly used in microwave engineering. To make the device easier to manufacture, a heavily doped GaAs layer replaced the metal layer below the active region. This waveguide design leads to similar guiding properties as a metal–semiconductor–metal confinement, at the expense of slightly higher calculated waveguide losses of 51 cm^{-1} instead of 38 cm^{-1}. Two structures with similar active regions have been grown. They consist of a 120 period GaAs/AlGaAs active region embedded between two highly doped $n \approx 5 \times 10^{18}\ \text{cm}^{-3}$ GaAs layers. A parabolic graded AlGaAs transition region has been introduced between the doped and undoped regions to enable an abrupt carrier distribution profile. The elementary cells of both active regions are very similar to the far-infrared vertical transition QC structure published previously.[7] However, small modifications have been made, in order to increase the current injection into the exited state. The injection barriers have respectively been reduced to 5.5 and 4.7 nm (instead of 6.0 nm) for samples S1683 and S1806. In order to compensate space charge accumulation in the structures, the first well of the injector has been doped with Si. Capacitance–voltage[9] measurements performed on the structures yield an average doping of $n = 3.4 \times 10^{15}\ \text{cm}^{-3}$ and $n = 7.4 \times 10^{15}\ \text{cm}^{-3}$ respectively. Compared to our first structure, the maximum injection current before appearance of the negative differential resistance region was increased from 40 to 100 A cm^{-2}, respectively, towards more than 700 A cm^{-2}. The extraction barriers have also been shortened from 4 nm down to 3 and 2.3 nm to enhance the extraction of the electrons from the lower level.

Conventional techniques usually applied to measure waveguide losses in semiconductor lasers[10–12] are not applicable in our case, as the observed luminescence intensity is too weak. The technique using a single, multisection device[13] is, however, feasible as it uses the luminescence generated by the QC structure inside the waveguide as the light source. In this configuration, separated electrical contacts of constant area are provided on top of the waveguide. The light intensity I_0 produced in a pumped section will travel down the waveguide to the edge of the sample with the intensity decreasing accordingly to the following relation:

$$I_t = I_0 e^{-\alpha_w L}, \tag{1}$$

where I_t is the transmitted light intensity measured at the edge of the waveguide, L is the optical path length measured from the pumped section to the sample edge, and α_w is the waveguide loss. The initial light intensity I_0, identical for all sections provided that they are pumped with same current, can be obtained by measuring the light intensity produced by

[a]Electronic mail: michel.rochat@unine.ch
[b]Electronic mail: jerome.faist@unine.ch

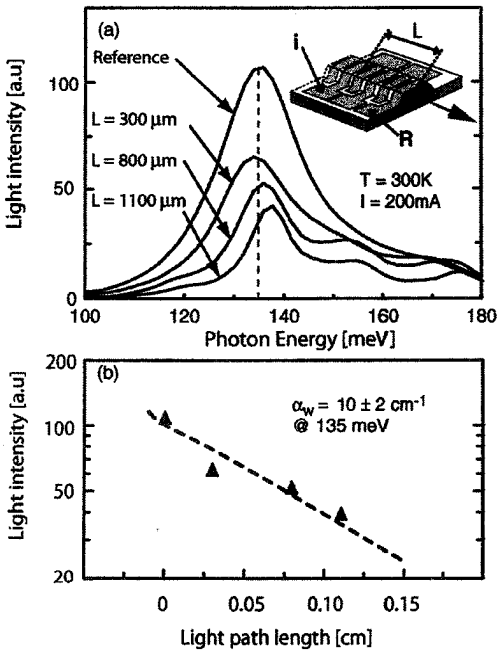

FIG. 1. (a) Mid-infrared luminescence spectra obtained for different optical path length, from a QC laser device working under laser threshold at room temperature. Inset is a view of the multisection injection processing of our samples. The optical path length is modified by sequentially pumping different sections (i) of the waveguide. (b) Reported intensities as a function of light path length are fitted to obtain the waveguide losses.

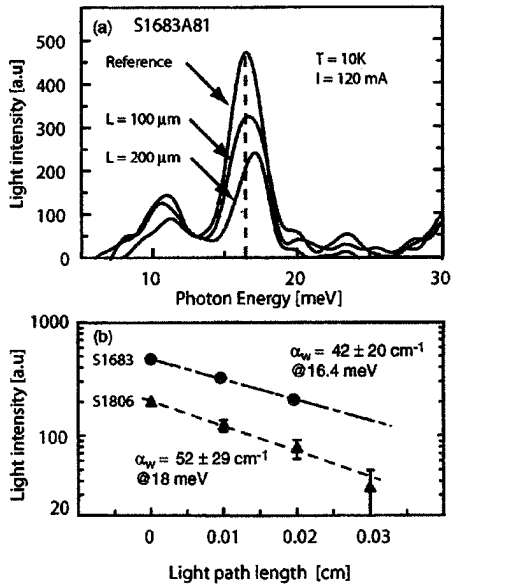

FIG. 2. (a) Obtained far infrared luminescence spectra from a double plasmon waveguide for various optical path lengths for similar sample processing as shown in inset of Fig. 1. (b) Reported intensities as a function of light path length for two active regions, emitting at 16.4 and 18 meV are presented.

pumping the front section [labeled R in inset Fig. 1(a)]. Pumping an other section of the waveguide changes the light path length. Practically this means removing the sample from the measuring setup and rewiring it. Initial alignment can therefore not be perfectly reproduced. This can be overcome by measuring both the transmitted light and the reference light intensity for each path length allowing further renormalization of the intensities. Waveguide losses are obtained by a fit to the renormalized intensities plotted versus light path. A slight complication to this method is that the sections are electrically not completely isolated from each other. A leakage current into the nominally unpumped sections might provide parasitic contributions to the luminescence. This leakage has the final effect to underestimate the true waveguide loss. These contributions can, however, be included in the function used for the fit.

To check the validity of the technique, waveguide loss measurements have first been performed on a state of the art 9.1 μm InGaAs/AlInAs mid-infrared quantum cascade laser with an epitaxial overgrowth by metalorganic vapor phase epitaxy of the InP top cladding and operated below the laser threshold.[14] The sample processing is similar to the one described later for far-infrared measurements. Spectral measurements have been performed at a constant current of 200 mA and at room temperature. Figure 1(a) shows the luminescence observed from the edge of the sample, for various light propagation lengths. All shown spectra have been renormalized to one common reference spectra. The peak intensity is plotted as a function of optical path length in Fig. 1(b). A fit to the optical data gives losses of 10 ± 2 cm^{-1}, which correspond well to the calculated loss of 9.5 cm^{-1}. In order to take into account the effect of the leakage current while injecting current into one section, we have measured the bias on the other ones. Current versus voltage curves performed for each section enabled us to obtain the current flow for each section. An exponential approximation for the current versus waveguide length was used as a corrective term in the fitting function, resulting into a 3% increase of the true waveguide losses.

For far-infrared waveguide loss measurements, 90 μm wide injection sections which had a separation of 10 μm between each other were deposited on top of 500 μm wide ridges by e-gun evaporation of Ti/Au (10/400 nm). To prevent device short circuiting due to lateral ridge current injection, a hard-baked resist layer has been used as an electrical insulator. Samples were soldered with indium on copper mounts and fixed on the cold finger of a He flow cryostat. The injected current was provided by a pulse generator programed to deliver bursts of 1.9 μs long pulses with a duty cycle of 80%. The repetition rate was limited by the time constant of our detector, leading to an overall duty cycle of 40%. The luminescence signal was collected by a wide numerical aperture gold-coated parabolic off-axis mirror and sent through a Fourier transform infrared spectrometer used in the step-scan mode. The resulting signal was then detected with a liquid helium cooled Si bolometer.[15]

Measurements have been performed in the far-infrared on samples S1683 and S1806. Data have been taken at a temperature of 10 K for both samples and with an injection current of 120 and 500 mA, respectively. Figure 2(a) shows the renormalized spectra for sample S1683. Similar results have been obtained for the other sample. An identical base line correction has been made to all the spectra in order to

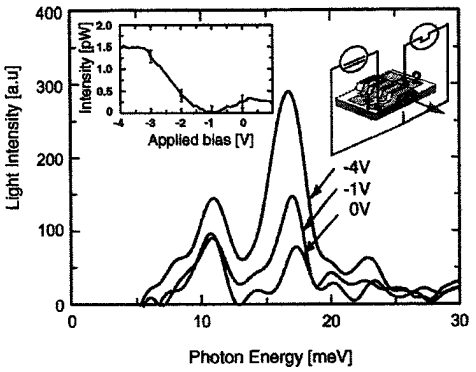

FIG. 3. Resonant absorption of the luminescence is demonstrated. Pulsed current injection is kept constant in section 2 and section 1 is either grounded or dc biased (right inset). The observed luminescence intensity leaving the waveguide increases with applied dc bias on the foremost section (left inset). Spectral measurements show a spectrally selective increase of the light intensity close to the emission energy, showing that this effect originates from the intersubband transition.

remove the blackbody emission due to sample heating. A decrease of the luminescence peak at 16.4 meV with increased light path length through the waveguide is clearly visible. However, the side peak at 12 meV does not show the same clear effect. It is thus attributed as an artifact occurring from the blackbody background. Luminescence intensity at 16.4 and 18 meV for samples S1683 and S1806 are plotted as a function of optical path [Fig. 2(b)]. Fits to the data, with the current leakage correction, give cavity losses of $\alpha_w = 42 \pm 20\,\mathrm{cm}^{-1}$ and $\alpha_w = 52 \pm 29\,\mathrm{cm}^{-1}$ for the two samples. Calculation of the losses based on free carrier absorption give according values of $\alpha_w = 51\,\mathrm{cm}^{-1}$ and $\alpha_w = 40\,\mathrm{cm}^{-1}$. The large error bars on our results originate mainly from the relatively low output power (typically less than 2 pW) in the edge configuration compared to the noise level. These low output powers also limit the range of light path lengths available to the experiment. Noise has been reduced by increased integration time (5 s per spectral point), but still remains important [nearly 10% of the most intense peak presented in Fig. 2(a)].

The structure, based on a vertical transition, does not exhibit significant Stark shift with applied voltage and will therefore show resonant reabsorption when the ground state is populated. This effect was not observed in our results presented earlier, because of current leakage, which always biases the front sections. Resonant reabsorption has, however, been observed when section 1 was either grounded or when a small dc voltage was applied while pulsed injection in section 2 was kept constant (left inset Fig. 3). Spectral measurements at various bias show that the optical transition is responsible for this effect, as a selective increase of the light intensity is observed at approximately the luminescence emission energy. Strictly speaking, we are therefore not measuring the waveguide losses at zero injected current, but the ones with which might always contain some small gain effect.

In conclusion, we have measured waveguide losses both in mid- and in far-infrared using a multisection single-pass technique. The waveguide losses obtained are in good agreement with calculated losses based on free carrier absorption. In the mid-infrared, the measured waveguide loss are lower than the Hakki–Paoli measurements published in the litterature,[16–18] with the exception of the recent work of Sirtori *et al.*[19] In the far-infrared, our results are very encouraging for future laser development based on the quantum cascade technology.

The authors would like to thank Daniel Hofstetter for fruitful discussions and proofreading the manuscript. This work was supported by the Swiss National Science Foundation.

[1] J. Faist, F. Capasso, D. L. Sivco, C. Sirtori, A. L. Hutchinson, and A. Y. Cho, Science **264**, 553 (1994).
[2] J. Faist, F. Capasso, D. L. Sivco, A. L. Hutchinson, S.-N. G. Chu, and A. Y. Cho, Appl. Phys. Lett. **72**, 680 (1998).
[3] A. Tredicucci, C. Gmachl, M. C. Wanke, F. Capasso, A. L. Hutchinson, D. L. Sivco, S.-N. G. Chu, and A. Y. Cho, Appl. Phys. Lett. **77**, 2286 (2000).
[4] M. Helm, P. England, E. Colas, F. DeRosa, and S. J. Allen, Jr., Phys. Rev. Lett. **63**, 74 (1989).
[5] B. S. Williams, B. Xu, Q. Hu, and M. R. Melloch, Appl. Phys. Lett. **75**, 2927 (1999).
[6] K. D. Maranowski, A. C. Gossard, K. Unterrainer, and E. Gornik, Appl. Phys. Lett. **69**, 3522 (1996).
[7] M. Rochat, J. Faist, M. Beck, U. Oesterle, and M. Ilegems, Appl. Phys. Lett. **73**, 3724 (1998).
[8] C. Sirtori, C. Gmachl, F. Capasso, J. Faist, D. L. Sivco, Albert L. Hutchinson, and A. Y. Cho, Opt. Lett. **23**, 1366 (1998).
[9] S. Blaser, M. Rochat, M. Beck, J. Faist, and U. Oesterle, Phys. Rev. B **61**, 8369 (2000).
[10] D. T. Cassidy, J. Appl. Phys. **56**, 3096 (1984).
[11] B. W. Hakki and T. L. Paoli, J. Appl. Phys. **46**, 1299 (1975).
[12] D. Hofstetter and J. Faist, IEEE Photonics Technol. Lett. **11**, 1372 (1999).
[13] J. D. Thomson, H. D. Summers, P. J. Hulyer, P. M. Smowton, and P. Blood, Appl. Phys. Lett. **75**, 2527 (1999).
[14] D. Hofstetter, M. Beck, T. Aellen, J. Faist, U. Oesterle, M. Ilegems, E. Gini, and H. Melchior, Appl. Phys. Lett. **78**, 1964 (2001), preceding paper.
[15] Optical calibration of our Si bolometer has been performed using a blackbody radiation source. Results have shown that the optical intensity of the luminescence published in Ref. 7 has to be increased by a factor of 7.7.
[16] C. Sirtori, J. Faist, F. Capasso, D. L. Sivco, A. L. Hutchinson, and A. Y. Cho, IEEE Photonics Technol. Lett. **9**, 294 (1997).
[17] C. Sirtori, J. Faist, F. Capasso, D. L. Sivco, A. L. Hutchinson, and A. Y. Cho, IEEE J. Quantum Electron. **33**, 89 (1997).
[18] A. Tredicucci, C. Gmachl, F. Capasso, D. L. Sivco, A. L. Hutchinson, and A. Y. Cho, Appl. Phys. Lett. **74**, 638 (1999).
[19] C. Sirtori, P. Kruck, S. Barbieri, H. Page, J. Nagle, M. Beck, J. Faist, and U. Oesterle, Appl. Phys. Lett. **75**, 3911 (1999).

Terahertz quantum-cascade laser operating up to 137 K

Benjamin S. Williams, Sushil Kumar, Hans Callebaut, and Qing Hu[a)]
Department of Electrical Engineering and Computer Science and Research Laboratory of Electronics, Massachusetts Institute of Technology, Cambridge, Massachusetts 02139

John L. Reno
Sandia National Laboratories, Department 1123, MS 0601, Albuquerque, New Mexico 87185-0601

(Received 25 August 2003; accepted 24 October 2003)

We report operation of a terahertz quantum-cascade laser at 3.8 THz ($\lambda \approx 79$ μm) up to a heat-sink temperature of 137 K. A resonant phonon depopulation design was used with a low-loss metal–metal waveguide, which provided a confinement factor of nearly unity. A threshold current density of 625 A/cm^2 was obtained in pulsed mode at 5 K. Devices fabricated using a conventional semi-insulating surface-plasmon waveguide lased up to 92 K with a threshold current density of 670 A/cm^2 at 5 K. © *2003 American Institute of Physics.* [DOI: 10.1063/1.1635657]

The extension of quantum-cascade laser (QCL)[1] operation from the mid-infrared into the underdeveloped terahertz frequency range (1–10 THz, 30–300 μm)[2–4] promises to provide new compact, coherent sources for applications such as spectroscopy, sensing, and imaging. At this early stage of development, high-temperature performance of terahertz QCLs is still rather limited, and cryogenic operation is required. For these lasers, the photon energy $\hbar\omega$ is smaller than the LO phonon energy ($E_{LO}=36$ meV in GaAs), and nonradiative relaxation via LO-phonon scattering is suppressed for cold electron distributions. However, at higher temperatures, thermally activated LO-phonon scattering dominates the upper state lifetime τ according to $\tau^{-1} \propto \exp[(\hbar\omega - E_{LO})/k_B T_e]$, where T_e is the electron temperature. As a result, the gain in terahertz QCLs has a much stronger temperature dependence than the gain in mid-infrared QCLs, where $\hbar\omega > E_{LO}$. For terahertz QCLs, operation has been obtained up to 103 K in pulsed mode and 68 K in cw mode in a bound-to-continuum design.[5,6] For chirped superlattice designs, lasing has been obtained at 74 K in pulsed mode, and 48 K in cw mode.[7] For both of these designs, depopulation of the lower radiative state takes place via intraminiband transport and scattering. High-temperature performance has been limited by various combinations of thermal backfilling of the lower radiative state from the injector, and reduction of the upper state lifetime due to thermally activated phonon scattering.

A different approach was taken for resonant phonon devices,[4,8] in which depopulation of the lower radiative state occurs via subpicosecond LO-phonon scattering. The large energy separation ($\geqslant E_{LO}$) between the injector states and the lower radiative state reduces thermal backfilling. Lasing was observed in pulsed mode up to 87 K,[9] but cw operation of this first design was not obtained, due to its relatively large threshold current density ($J_{th} > 800$ A/cm^2). The large J_{th} did not necessarily reflect a weak gain or high optical loss, but rather it was inflated by the presence of a strong parasitic current channel.[10]

In this letter, we report lasing up to a heat-sink temperature of $T_{max}=137$ K in a resonant phonon structure [shown in Fig. 1(a)] that is very similar to the one reported in Ref. 4, except that the 24 Å intra-injector barrier was thickened to 30 Å. This change narrowed the 2-1 injector anticrossing from $\Delta_{21}=6.5$ meV to $\Delta_{21}=5.0$ meV. The intent was for a tighter injection doublet to provide more selective injection into the upper radiative state $n=5$. In addition, below the design bias, the thicker barrier reduces the coupling between the injector state $n=1'$ and the excited state $n=3$ in the wide well of the next module, which was the cause of the aforementioned parasitic current channel.

The structure, labeled FL178C-M1, was grown by molecular-beam epitaxy on a semi-insulating (SI) GaAs substrate with 178 cascaded modules. Cladding and contact layers were grown as in Ref. 11, except that the undoped

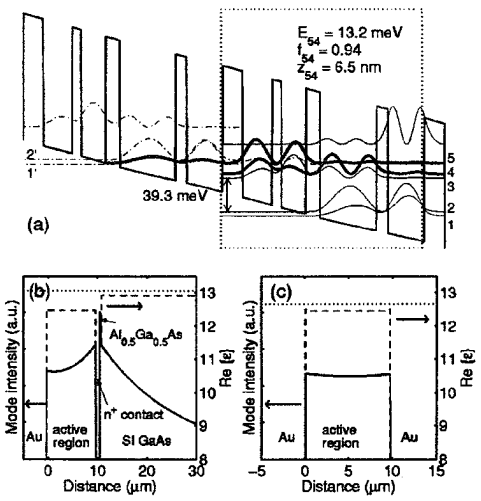

FIG. 1. (a) Conduction band profile calculated using a self-consistent Schrödinger and Poisson solver (72% band offset). The four-well module grown in GaAs/$Al_{0.15}Ga_{0.85}As$ is outlined by the dotted box. Beginning with the left injection barrier, the layer thicknesses in Å are 54/78/24/65/38/149/30/95. The 149 Å well is doped at $n=1.9\times10^{16}$ cm^{-3}, which yields a sheet density of $n=2.8\times10^{10}$ cm^{-2} per module. Also shown are the mode profiles (solid lines) and the real part of the dielectric constant $\epsilon(\omega)$ (dashed lines) for (b) SISP and (c) metal–metal waveguides.

a)Electronic mail: qhu@mit.edu

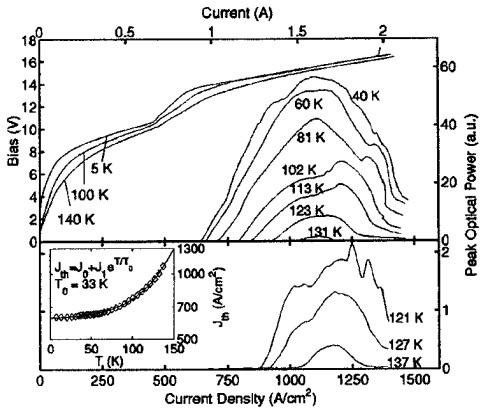

FIG. 2. Emitted light and bias versus current at various temperatures for metal–metal devices measured using 200 ns pulses repeated at 1 kHz. The $L-I$ characteristics in the upper panel are measured from a 60-μm-wide, 2.48-mm-long ridge. The $V-I$ characteristic is measured using a smaller structure (100 μm wide, 1.45 mm long). The lower panel displays $L-I$ characteristics from a 150-μm-wide, 2.74-mm-long ridge, along with its threshold current density versus temperature (inset). Note that the current axis is only applicable to the 60-μm-wide device.

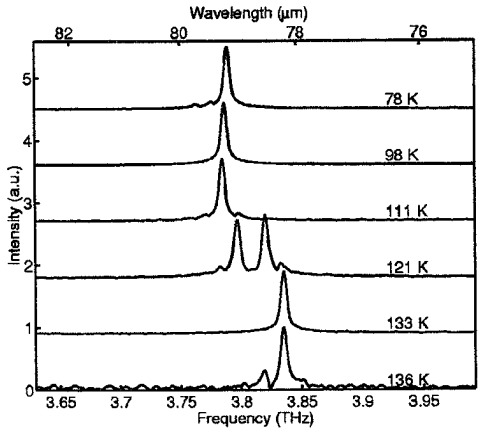

FIG. 3. Spectra from a 100-μm-wide, 2.74-mm-long metal–metal ridge taken at various heat-sink temperatures using 200 ns pulses repeated at 5 kHz, all biased at approximately the same current densities of 1170–1200 A/cm^2. A Nicolet 850 Fourier transform spectrometer was used with a Ge:Ga photodetector. The linewidth is limited by the spectrometer resolution (0.125 cm^{-1}).

$Al_{0.5}Ga_{0.5}As$ etch-stop layer was 0.3 μm thick, and the lower n^+ GaAs contact layer was 0.8 μm thick and doped at 3×10^{18} cm^{-3}. This device was fabricated into a low-loss, high-confinement metal–metal waveguide using In–Au metallic wafer bonding as described in Ref. 11, and ridges were dry etched using the top Ti/Au (200/4000 Å) metallization as a self-aligned etch mask. Devices were also processed into SI surface-plasmon (SISP) waveguides using wet etching, as described in Ref. 4. For the SISP devices only, a high-reflectivity (HR) coating (Al_2O_3/Ti/Au) was evaporated on the cleaved rear facet. One-dimensional mode profiles were calculated for the two waveguides, and are shown in Figs. 1(b) and 1(c). At 3.8 THz, a waveguide loss of $\alpha_w = 14.2$ cm^{-1} and a confinement factor of $\Gamma = 0.98$ were obtained for the metal–metal waveguide, while $\alpha_w = 8.2$ cm^{-1} and $\Gamma = 0.324$ were obtained for the SISP guide. Drude-model relaxation times of 0.1, 0.5, and 0.05 ps were used for the heavily doped semiconductor, lightly doped semiconductor, and gold, respectively.

The highest operating temperatures were observed from the metal–metal waveguide devices. Light versus current ($L-I$) characteristics taken from typical devices are shown in Fig. 2. A 150-μm-wide, 2.74-mm-long Fabry–Pérot ridge lased up to a heat-sink temperature of $T_{max}=137$ K when biased with 200 ns pulses repeated at 1 kHz. This device displayed a threshold current density of $J_{th}=625$ A/cm^2 at 5 K. In addition, a 60-μm-wide, 2.48-mm-long ridge lased up to 131 K, with $J_{th}=630$ A/cm^2 at 5 K. Voltage versus current ($V-I$) characteristics are also shown from a similar, but smaller device (100 μm wide, 1.45 mm long). In these devices, lasing occurs up to a peak current density of $\sim$1400 A/cm^2, whereupon the injector subband $n=1'$ becomes misaligned with the upper radiative state $n=5$, and negative differential resistance is observed. The shoulder in the $V-I$ at approximately 500 A/cm^2 ($\sim$10 V) corresponds to the previously mentioned parasitic current channel;[10] electrons are not injected into the upper radiative state until the device is biased beyond this point. Indeed, lasing begins at a current density only slightly higher than this parasitic channel, which indicates that J_{th} is still limited by the parasitic channel rather than by intrinsic gain or loss. Compared to the previous design, in which the lowest obtained threshold was $J_{th}=806$ A/cm^2, increasing the intra-injector barrier thickness suppressed the parasitic channel and reduced J_{th}. A plot of J_{th} versus heat-sink temperature is shown in the inset of Fig. 2, along with a fit to the phenomenological relation $J_{th}=J_0+J_1\exp(T/T_0)$. The extracted characteristic temperature is $T_0=33$ K. This value is significantly smaller than those for mid-infrared QCLs, which are typically greater than 100 K. Using ridges of different widths did not affect device performance very much. In addition to the devices mentioned earlier, a 100-μm-wide ridge and an 80-μm-wide ridge of the same length (2.74 mm) displayed $T_{max}=136$ and 131 K, respectively. In addition, a circular device with a 400 μm diameter lased in a whispering gallery mode with $T_{max}=105$ K.

The sharp feature in the $V-I$ associated with the parasitic channel ($\sim$10 V) is likely an indication that high-field domains have developed, and individual modules or groups of modules have "jumped" to higher biases to maintain constant current. This is an unintended side effect of tightening the injection doublet. Even though most modules return to their correct alignment as the bias is increased past the high differential resistance region, there is no guarantee that all modules will be correctly biased. In fact, the threshold bias voltage of $\sim$14 V is much higher than the designed value of 178×64 mV$\approx$11.4 V, which indicates that many modules are probably biased at much higher voltages than designed. Hence, injector design should be optimized to further suppress the parasitic channel and prevent high-field domain formation.

Pulsed spectra taken at up to 136 K from a 100-μm-wide, 2.74-mm-long Fabry–Pérot ridge structure are shown in Fig. 3. Lasing was seen at approximately 3.8 THz, which corresponds to a wavelength of $\lambda\approx79$ μm and a photon en-

ergy of 15.7 meV. This is somewhat higher than the 14 meV photon energy observed for the device in Refs. 4 and 9. This is consistent with high-field domain development, in which modules jump to higher bias points than they otherwise might so that the separation E_{54} is increased due to Stark shift. The observed frequency shift at different temperatures is not due to temperature tuning, but rather due to mode-hopping caused by the shift of the gain curve at slightly different bias points. The spontaneous emission linewidth is measured to be 6 meV ($\sim$1.5 THz). The line shape is far different from a Lorentzian, and this broad linewidth is likely due to non-uniform alignment of different modules.

As observed previously,[11] the metal–metal waveguide devices lased only for approximately the first 10–30 μs of an applied pulse. This is attributed to rapid heating of the active region caused by a large thermal resistance at the bonding interface. This phenomenon has been observed in similar metal–metal waveguide QCLs that operated in the mid-infrared.[12] Improvements in bonding layer quality should alleviate this problem.

Devices fabricated using SISP waveguides were also tested, but did not achieve the same high-temperature performance as their metal–metal counterparts. A 150-μm-wide, 2.97-mm-long ridge with a HR-coated rear facet obtained T_{max}=92 K, with J_{th}=670 A/cm^2 at 5 K. A peak collected power of approximately 2.5 mW was observed in pulsed mode from a 150-μm-wide, 1.5-mm-long, HR-coated ridge. The lower T_{max} of the SISP device is primarily due to the extra loss and low confinement factor Γ. A small value of Γ inflates the effect of the mirror losses α_m, since the total threshold gain is given by $g_{th}=(\alpha_w+\alpha_m)/\Gamma$. In addition, the mirror losses are further reduced for metal–metal waveguides due to the increased facet reflectivity caused by the impedance mismatch between the tightly confined mode and free space. Current spreading in the wet-etched SISP devices may also have reduced the available gain.[9] However, heat removal for these structures was much better than for the metal–metal devices. For a 150-μm-wide, 1.5-mm-long, HR-coated ridge, cw operation was briefly observed for several seconds at 13 K before heat buildup in the cryostat stopped operation.

Monte Carlo simulations of active region transport and gain were performed as described in Ref. 10 and are consistent with the experimental results. As shown in Fig. 4, the calculated peak gain declines as the lattice temperature T_l rises above $\sim$80 K and τ_5 decreases due to thermal activation of LO-phonon scattering from $n=5$ into $n=3$ and 4. The simulation results indicate that for T_l below $\sim$80 K, the electron temperature T_e is not very sensitive to T_l, whereas above $\sim$80 K, T_e tracks T_l with a temperature difference ($\sim$20–60 K) that depends on the subband. At $T_l>80$ K, cooling due to intrasubband LO-phonon scattering becomes efficient, keeping T_e not too much above T_l.[13] From the calculated losses, which were approximated as temperature independent, we can estimate the maximum operating temperature of the laser to be $\sim$85 K for a SISP waveguide, and $\sim$160 K for a metal–metal waveguide. These values correspond reasonably well with the measured maximum temperatures of 92 and 137 K, respectively.

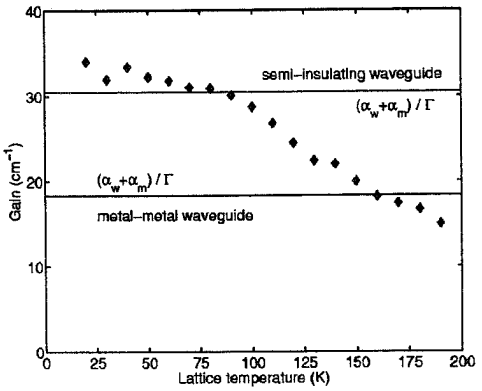

FIG. 4. Maximum available gain versus lattice temperature calculated with a Monte Carlo solver, compared with calculated threshold gain required for metal–metal and SISP waveguide.

In conclusion, we have extended the temperature range for lasing in resonant phonon terahertz QCLs by improving injection and reducing waveguide losses. Redesign of the injector region should prevent the development of high-field domains (which will result in a narrower linewidth and more modules contributing to gain), and should further reduce the parasitic current channel, which would allow lower thresholds and even higher temperature operation. Improvements in metallic wafer bonding and heat-sinking for metal–metal waveguides will allow for more robust cw operation.

The authors acknowledge R. Köhler and A. Tredicucci for helpful discussions. This work is supported by AFOSR, NASA, and NSF. Sandia is a multiprogram laboratory operated by Sandia Corporation, a Lockheed Martin Company, for the United States Department of Energy under Contract DE-AC04-94AL85000.

[1] J. Faist, F. Capasso, D. L. Sivco, C. Sirtori, A. L. Hutchinson, and A. Y. Cho, Science **264**, 553 (1994).
[2] R. Köhler, A. Tredicucci, F. Beltram, H. E. Beere, E. H. Linfield, A. G. Davies, D. A. Ritchie, R. C. Iotti, and F. Rossi, Nature (London) **417**, 156 (2002).
[3] M. Rochat, L. Ajili, H. Willenberg, J. Faist, H. Beere, G. Davies, E. Linfield, and D. Ritchie, Appl. Phys. Lett. **81**, 1381 (2002).
[4] B. S. Williams, H. Callebaut, S. Kumar, Q. Hu, and J. L. Reno, Appl. Phys. Lett. **82**, 1015 (2003).
[5] G. Scalari, L. Ajili, J. Faist, H. Beere, E. Linfield, D. Ritchie, and G. Davies, Appl. Phys. Lett. **82**, 3165 (2003).
[6] J. Faist (personal communication).
[7] R. Köhler, A. Tredicucci, F. Beltram, H. E. Beere, E. H. Linfield, A. G. Davies, D. A. Ritchie, S. S. Dhillon, and C. Sirtori, Appl. Phys. Lett. **82**, 1518 (2003).
[8] M. A. Stroscio, M. Kisin, G. Belenky, and S. Luryi, Appl. Phys. Lett. **75**, 3258 (1999).
[9] B. S. Williams, S. Kumar, H. Callebaut, Q. Hu, and J. L. Reno, Electron. Lett. **39**, 915 (2003).
[10] H. Callebaut, S. Kumar, B. S. Williams, Q. Hu, and J. L. Reno, Appl. Phys. Lett. **83**, 207 (2003).
[11] B. S. Williams, S. Kumar, H. Callebaut, Q. Hu, and J. L. Reno, Appl. Phys. Lett. **83**, 2124 (2003).
[12] K. Unterrainer, R. Colombelli, C. Gmachl, F. Capasso, H. Y. Hwang, A. M. Sergent, D. L. Sivco, and A. Y. Cho, Appl. Phys. Lett. **80**, 3060 (2002).
[13] J. Shah, in *Hot Carriers in Semiconductor Nanostructures*, edited by J. Shah (Academic, San Diego, 1992), Chap. IV.1, pp. 169–188.